SciVerse
ScienceDirect

Hub | **ScienceDirect** | Scopus | SciTopics | Applications

Home   Browse   Search   My settings   My alerts   Shopping cart

Articles ⊙   All fields [_____]   Author [_____]
Images ○   Journal/Book title [_____]   Volume [__]   Issue [__]   Page [__]   Se

Saccelrys® | IDC Manufacturing Insights Whitepaper: Designing Environmental Sustainability into Product Research and Develop

PDF (399 K)   Export citation   E-mail article

Article   Figures/Tables (18)   References (18)   Thumbnails | Full-Size images

BEM analysis of thermal and mechanical shock in a two-dimensional finite domain considering coupled thermoelasticity

P. Hosseini-Tehrani, M.R. Eslami 🔺, ✉

 Mechanical Engineering Department, Amirkabir University of Technology, P.O. Box 15875-4413, Hafez Avenue No. 424, Tehran 15914, Iran

Abstract

A boundary element method based on the Laplace-transform technique is developed for transient coupled thermoelasticity problems of two-dimensional finite domain. The Laplace-transform method is applied to the time domain and the resulting equations in the transformed field are discretized using the boundary element method. The nodal dimensionless temperature and displacements in the transformed domain are inverted to obtain the actual physical quantities, using the numerical inversion of the Laplace-transform method. The

work is concerned with the thermal and mechanical shocks in a finite domain considering classical coupled theory of thermoelasticity. Elastic and thermoelastic wave creation and propagation in a finite domain and their effects on each other are investigated. Numerical implementations are presented and compared with the known data.

Keywords: Thermal and mechanical shock; Coupled thermoelasticity; Two-dimensional finite domain

Article Outline

1. Introduction
2. Governing equations
3. Boundary integral equation
4. Fundamental solution
5. Results and discussion
6. Conclusions

References

1. Introduction

In recent years, considerable attention has been paid to the numerical analysis of coupled thermoelasticity problems, which have a wide range of applications in engineering and science. Coupled thermoelasticity encompasses the phenomena that describe the elastic and thermal behavior of solids and their interactions under mechanical and thermal loadings. Many attempts have been directed toward the solution of uncoupled thermoelasticity problems in steady or transient heat conduction states, but few investigations have been done successfully for coupled thermoelasticity problems of engineering structures. Analytical solutions for some dynamic problems in coupled thermoelasticity of half-space were obtained by Danilovskaya [1] and [2], and Strengberg and Chakravorty [3]. For some of the quasi-static problems in coupled thermoelasticity, Boley and Tolins [4] obtained analytical solutions; whereas Nickell and Sackman [5] presented approximate solutions. The boundary element method (BEM), recognized in recent years as a powerful tool in numerical analysis, was applied by Rizzo and Shippy [6] to the BEM solution of transient uncoupled problems. We may also refer to Tanaka et al. [7], and Sladek and Sladek [8]. The BEM for the coupled problem in thermoelasticity with numerical computation have been reported by Suh and Tosaka [9], Ishiguro and Tanaka [10], and Dargush and Banerjee [11]. Suh and Tosaka used the Laplace transform, while Ishiguro and Tanaka proposed a BEM based on the time-stepping approximation of time derivatives. Dargush and Banerjee presented a BEM solution implementing a reciprocal theorem for quasi-static poroelasticity or thermoelasticity problems of steady-state thermoelasticity problems.

Hector and Kim [12] investigated transient temperature distribution in a two-dimensional isotropic medium using the hyperbolic heat conduction model for an extremely short time period and showed dissipating energy upon reflection at the boundaries. Wagner [13] presented the fundamental matrix of the system of partial differential operator that governs the dynamic behavior of heat and strain in elastic medium by simple definite integrals and power series in one dimension. Chen and Dargush [14] used a BEM for transient and dynamic problems in generalized thermoelasticity in a half-space by using the Laplace-transform method. Hosseini Tehrani and Eslami [15] showed the coupling effects in natural frequencies, temperature distribution, and resonance amplitudes in a time harmonic problem by BEM.

Recently, the authors presented a general overview of the problem of generalized coupled thermoelasticity in finite domain using the Laplace-transform method in time domain. The aim of the paper was to establish

their mathematical modeling and to study the main differences between the response of the solution domain under thermal shock loading alone for different coupled thermoelastic assumptions. The classical coupled thermoelasticity (CCT), versus the Lord–Shulman (LS) and Green–Lindsay (GL), models were checked and the result were compared. Due to the vast knowledge inherent in the problem, it is intended to investigate each model, i.e. CCT, LS, and GL models, separately. In the comprehensive study of each of these individual models the behavior of the model under thermal shock loading versus the mechanical shock loading is studied. The behavior of the displacement, temperature, and stress distribution by time and the wave fronts for two different loadings are discussed. The very interesting conclusion drawn from this comprehensive study is the magnitude of the wave fronts produced by each type of loadings compared to the uncoupled theory. The result of this paper is further improved using a quadratic boundary element formulation, unlike the paper in Hosseini Tehrani and Eslami [16] which is based on constant element formulation.

In this paper, a Laplace-transform boundary element method is developed for the dynamic problem of coupled thermoelasticity. The boundary element formulation for dynamic coupled thermoelasticity problems in two-dimensional finite domain is presented and a single heat excitation is used to derive the boundary element formulations. Aspects of numerical implementation are discussed. This implementation permits the solution of transient dynamic coupled problems, while requiring only surface discretization. Temperature and traction loading is used to show conceptually what is involved in the coupled theory of thermoelasticity. The thermo-mechanical waves production and propagation are investigated and the influence of coupling parameter in stress, temperature, and displacement distribution is discussed.

The important features of this paper compared to the previous publications of the authors and other related papers are the considerations of the higher order boundary element formulation, the interaction of the mechanical and thermal shock loads in the stress distribution around the wave front, and the unique treatments of the problem in finite space and time domain. These are discussed in 5 and 6. Throughout this paper, the summation convention on repeated indices is used. A dot indicates time differentiation and the subscript i after a comma shows the partial differentiation with respect to x_i (i=1,2).

2. Governing equations

A homogeneous isotropic thermoelastic solid is considered. In the absence of body forces and heat flux, the governing equations for the dynamic coupled thermoelasticity in the time domain can be written as follows:

$$(\lambda + \mu)\, u_{j,ij} + \mu\, u_{i,jj} - \rho\, \ddot{u}_i - \gamma\, T_{,i} = 0, \tag{1}$$

$$k T_{,ii} - \rho c_e \dot{T} - \gamma T_0 \dot{u}_{j,j} = 0 \tag{2}$$

where λ, μ, u_i, ρ, T, T_0, k, γ and c_e are Lame's constants, the components of displacement vector, density, absolute temperature, reference temperature, conductivity, stress–temperature modulus and specific heat, respectively. It is convenient to introduce the dimensionless variables as follows:

$$\hat{x} = \frac{x}{\alpha}; \quad \hat{t} = \frac{t C_1}{\alpha}; \quad \hat{\sigma}_{ij} = \frac{\sigma_{ij}}{\gamma T_0}; \quad \hat{u}_i = \frac{(\lambda + 2\mu)\, u_i}{\alpha \gamma T_0}; \quad T = \frac{T - T_0}{T_0} \tag{3}$$

where $\alpha = k/\rho c_e C_1$ is the dimensionless unit length and $C_1 = \sqrt{(\lambda + 2\mu)/\rho}$ the velocity of propagation of the longitudinal wave. (1) and (2) take the form (dropping the hat for convenience)

$$\tag{4}$$

$$\frac{\mu}{\lambda+2\mu}u_{i,jj} + \frac{\lambda+\mu}{\lambda+2\mu}u_{j,ij} - T_{,i} - \ddot{u}_i = 0,$$

$$T_{,ii} - \dot{T} - \frac{T_0\gamma^2}{\rho c_e(\lambda+2\mu)}\dot{u}_{j,j} = 0. \tag{5}$$

Transferring (4) and (5) to the Laplace domain yields

$$\frac{\mu}{\lambda+2\mu}u_{i,jj} + \frac{\lambda+\mu}{\lambda+2\mu}u_{j,ij} - T_{,i} - s^2 u_i = 0, \tag{6}$$

$$T_{,ii} - sT - \frac{T_0\gamma^2}{\rho c_e(\lambda+2\mu)}su_{j,j} = 0. \tag{7}$$

(6) and (7) are rewritten in matrix form as

$$L_{ij}\,U_j = 0. \tag{8}$$

For the two-dimensional domain, the operator L_{ij} reduces to

$$L_{ij} = \begin{bmatrix} \dfrac{\mu}{\lambda+2\mu}\Delta + \dfrac{\lambda+\mu}{\lambda+2\mu}D_1^2 - s^2 & \dfrac{\lambda+\mu}{\lambda+2\mu}D_1 D_2 & -D_1 \\[2ex] \dfrac{\lambda+\mu}{\lambda+2\mu}D_1 D_2 & \dfrac{\mu}{\lambda+2\mu}\Delta + \dfrac{\lambda+\mu}{\lambda+2\mu}D_2^2 - s^2 & -D_2 \\[2ex] -\dfrac{T_0\gamma^2}{\rho c_e(\lambda+2\mu)}sD_1 & -\dfrac{T_0\gamma^2}{\rho c_e(\lambda+2\mu)}sD_1 & \Delta - s \end{bmatrix},$$

$$U_i = \begin{bmatrix} u_1 & u_2 & T \end{bmatrix}$$

where $D_i = \partial/\partial x_i$ ($i=1,2$) and Δ denotes the Laplacian. The boundary conditions are assumed to be as follows:

$$u_i = \bar{u}_i \quad \text{on } \Gamma_u, \tag{9}$$
$$\tau_i = \bar{\tau}_i = \sigma_{ij}n_j \quad \text{on } \Gamma_\tau,$$
$$T = \bar{T} \quad \text{on } \Gamma_T,$$
$$q = \bar{q}_n = q_i n_i \quad \text{on } \Gamma_q$$

where $\bar{u}, \bar{\tau}_i, \bar{T}$, and $\bar{q}$ are the specified displacement, traction, temperature, and heat flux vector on the boundary.

3. Boundary integral equation

In order to derive the boundary integral problem, we start with the following weak formulation of the differential equation set (8) for the fundamental solution tensor V_{ik}^*:

$$\int_\Omega (L_{ij}\,U_j)\,V_{ik}^*\,d\Omega = 0. \tag{10}$$

After integrating by parts over the domain and taking a limiting procedure approaching the internal source point to the boundary point, we can obtain the following boundary integral equation:

$$C_{kj} U_k(y,s) = \int_\Gamma T_\alpha(x,s) V^*_{\alpha j}(x,y,s) - U_\alpha(x,s)\Sigma^*_{\alpha j}(x,y,s)\, d\Gamma(x) + \int_\Gamma T_{,n}(x,s) \tag{11}$$

where $U_\alpha = u_\alpha$ ($\alpha = 1,2$) and $U_3 = T$, and C_{kj} denotes the shape coefficient tensor. The kernel $\Sigma^*_{\alpha j}$ in Eq. (11) is defined by

$$\Sigma^*_{\alpha j} = \left[\left(\frac{\lambda}{\lambda + 2\mu} V^*_{kj,k} + \frac{T_0\gamma^2}{\rho\, C_e(\lambda + 2\mu)} s V^*_{3j} \right) \delta_{\alpha\beta} + \frac{\mu}{\lambda + 2\mu}(V^*_{\alpha j,\beta} + V^*_{\beta j,\alpha}) \right] n\beta. \tag{12}$$

Here the fundamental solution tensor V_{jk} must be determined as the tensor which satisfies the differential equation:

$$l_{ij} V^*_{jk} = -\delta_{ik}\delta(x-y) \tag{13}$$

where l_{ij} is the adjoint operator of L_{ij} in Eq. (8) and is given by:

$$l_{ij} = \begin{bmatrix} \dfrac{\mu}{\lambda + 2\mu}\Delta + \dfrac{\lambda + \mu}{\lambda + 2\mu} D_1^2 - s^2 & \dfrac{\lambda + \mu}{\lambda + 2\mu} D_1 D_2 & -\dfrac{T_0\gamma^2}{\rho c_e(\lambda + 2\mu)} \\[2mm] \dfrac{\lambda + \mu}{\lambda + 2\mu} D_1 D_2 & \dfrac{\mu}{\lambda + 2\mu}\Delta + \dfrac{\lambda + \mu}{\lambda + 2\mu} D_2^2 + s^2 & -\dfrac{T_0\gamma^2}{\rho c_e(\lambda + 2\mu)} \\[2mm] -D_1 & -D_2 & \Delta - s \end{bmatrix}$$

4. Fundamental solution

In order to construct the fundamental solution, we put the fundamental solution tensor V^*_{ij} of Eq. (13) in the following potential representation by using the transposed co-factor operator μ_{ij} of l_{ij} and scalar function Φ^* [17]:

$$V^*_{ij}(x,y,s) = \mu_{ij}\Phi^*(x,y,s). \tag{14}$$

After substitution of Eq. (14) into Eq. (13), we obtain the following differential equations:

$$\Lambda\Phi^* = -\delta(x-y) \tag{15}$$

where

$$\Lambda = \det(l_{ij}) = \frac{\mu}{\lambda + 2\mu}(\Delta - h_1^2)(\Delta - h_2^2)(\Delta - h_3^2) \tag{16}$$

and h_i^2 are

$$h_1^2 = \frac{\lambda + 2\mu}{\mu}s^2, \quad h_2^2 + h_3^2 = s^2 + s\left(1 + \frac{T_0\gamma^2}{\rho\, C_e(\lambda + 2\mu)}\right), \quad h_2^2 h_3^2 = s^3. \tag{17}$$

Here, h_1 is the longitudinal wave velocity, h_2 the thermal wave velocity, and h_3 the rotational wave velocity; and

$$\Phi^* = \frac{\lambda + 2\mu}{2\pi\mu} \left[\frac{K_0(h_1 r)}{(h_2^2 - h_1^2)(h_3^2 - h_1^2)} + \frac{K_0(h_2 r)}{(h_3^2 - h_2^2)(h_1^2 - h_2^2)} + \frac{K_0(h_3 r)}{(h_1^2 - h_3^2)(h_2^2 - h_3^2)} \right] \tag{18}$$

where K_0 is the modified Bessel function of second kind and zero order. The fundamental solution tensor V_{ij}^* for the two-dimensional domain is found as follows:

$$V_{\alpha\beta}^* = \sum_{k=1}^{3} (\psi_k(r)\delta_{\alpha\beta} - \kappa_k r_{,\alpha} r_{,\beta}) \quad (\alpha,\beta = 1,2), \qquad V_{3\alpha}^* = \sum_{k=1}^{3} \xi_k'(r) r_{,\alpha}, \qquad V_{\alpha 3}^* = \sum_k \tag{19}$$

where

$$\psi_k(r) = \frac{W_k}{2\pi} \left[(h_k^2 - m_2)(h_k^2 - m_1) + \left(\frac{\lambda + \mu}{\mu} \right)\left(h_k^2 - m_1 \left(1 + C\frac{\lambda + 2\mu}{\lambda + \mu} \right) \right) \right] h_k^2 \tag{20}$$

$$+ \frac{W_k(\lambda + \mu)}{2\pi\mu} \left[h_k^2 - m_1 \left(1 + C\frac{\lambda + 2\mu}{\lambda + \mu} \right) \right] \frac{h_k}{r} K_1(h_k r), \qquad \kappa_k(r) = \frac{W_k(\lambda + \mu)}{2\pi\mu} \left[h \right.$$

$$= \frac{W_k}{2\pi} \left(h_k^2 - \frac{\lambda + 2\mu}{\mu} s^2 \right) h_k K_1(h_k r), \qquad \xi_k(r) = \frac{W_k}{2\pi} Cs \left(h_k^2 - \frac{\lambda + 2\mu}{\mu} s^2 \right) h_k K_1(l$$

and

$$r = \|x - y\|; \qquad m_1 = s; \qquad m_2 = \frac{\lambda + 2\mu}{\mu} s^2; \qquad C = \frac{T_0 \gamma^2}{\rho c_e (\lambda + 2\mu)}; \qquad W_i = \frac{-}{(h_i^2 - h_j^2)(} \tag{21}$$

where K_0, K_1 and K_2 are the modified Bessel functions of second kind and zero, first, and second order, respectively.

In order to solve numerically the boundary element integral equation (11), the standard boundary element procedure may be applied. When transformed numerical solutions are specified, transient solutions are obtained using an appropriate numerical inversion technique. In this paper, the method presented by Durbin [18] is adopted for this numerical inversion.

5. Results and discussion

To compare the two-dimensional results of the method presented in this paper with the results of the available data, coupled thermoelasticity of a half-space is considered. The boundary element solution and the analytical solution of the coupled and uncoupled thermoelasticity of a half-space are given by Chen and Dargush [14] and Sternberg and Chakravorty [3], respectively. Both solutions are based on the Laplace-transform method.

To model a half-space subjected to thermal shock, a square plate subjected to heating at one edge with a step function for the temperature rise is considered (Fig. 1). The plate is thermally isolated and is traction

free at the other three edges. The results are obtained along the axis of symmetry of the plate (the *x*-axis). The plate length is considered 10 (non-dimensional), and the results are obtained at *x*=1 (non-dimensional). With this *l/x* ratio, finite domain's results have very good agreement with the half-space problem at the early stages of thermal shock application. Fig. 2, Fig. 3 and Fig. 4 show a comparison of the dimensionless temperature, axial displacement, and axial stress at dimensionless length *x*=1 (which is the location of the elastic wave front at the non-dimensional time *t*=1). The results are plotted for the analytical solution [3], the boundary element solution [14], and the present results for different coupling parameters. The case of *C*=0 corresponds to the uncoupled solution. The coupled results are presented for *C*=1 to match the results of Chen and Dargush [14]. This value is unrealistically high for the material of interest. It is seen that the axial displacement, temperature, and axial stress results of the presented paper have good agreement with the analytical and boundary element solutions for the uncoupled and coupled cases.

Full-size image (2K)
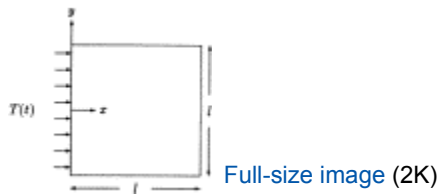
Fig. 1.

A square plate subjected to thermal loading.

Full-size image (9K)
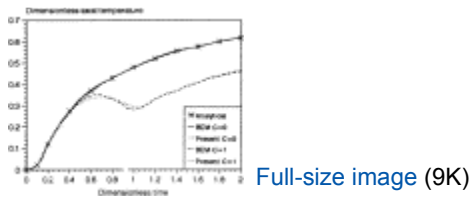
Fig. 2.

Comparison of the dimensionless temperature at *x*=1.

Full-size image (10K)
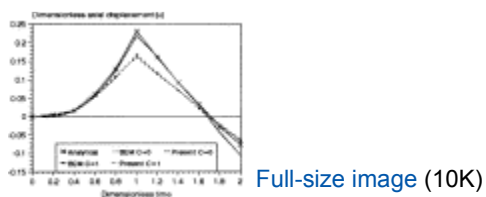
Fig. 3.

Comparison of the dimensionless axial displacement at *x*=1.

[Full-size image](#) (8K)
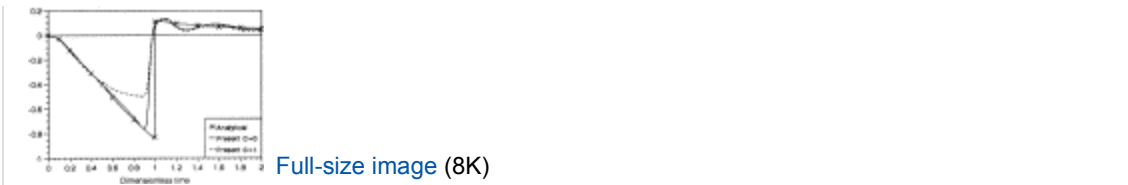
Fig. 4.

Comparison of the dimensionless axial stress at $x=1$.

Now, consider a square plate of isotropic and homogeneous material. The dimensionless size of the plate is $l=10$, and is of unit thickness, as shown in Fig. 5. The mechanical and thermal boundary conditions are

$$u_1 = u_2 = 0 \text{ at } x = 10; \quad \tau_i = 0 \text{ at } y = \pm 5, \quad T_{,1} = 0 \text{ at } x = 10; \quad T_{,2} = 0 \text{ at } y = : \tag{22}$$

where τ_i are the traction components. The edge $x=0$ is kinematically free and thermally exposed to a temperature or pressure shock with the known equation

$$T(t) = 5\,t\exp(-2t), \tag{23}$$

$$\tau_1 = 5\,t\exp(-2t) \tag{24}$$

where t is the dimensionless time. When thermal shock is applied to the edge $x=0$, $\tau_i=0$ on $x=0$. Temperature shock is in the form of heat input (Fig. 6), and pressure shock is applied in the positive x-direction. Three cases of loadings are considered:

1. *Thermal shock alone:* The temperature shock of Eq. (23) is applied to the edge $x=0$. We consider the uncoupled equations ($C=0$) and study the accuracy of the boundary element solution by assuming the constant and quadratic elements. The boundary of the plate is divided into 40 and 20 number of elements for the constant and quadratic elements, respectively. Fig. 7, Fig. 8 and Fig. 9 show the comparison of the temperature T, axial displacement u, and the axial stress σ_{xx} along the x-axis at dimensionless time $t=3$ and $t=6$. The figures show that the constant elements over-estimates the temperature distribution especially for the longer x-values and under-estimate the x-values axial displacement and the stress distribution. It is clearly shown that the constant elements approach is not capable to represent the sharp variation of stress near the free edge at $x=0$, and its error in temperature distribution increases with the increase of the distance from the free edge $x=0$, where the temperature shock is applied. We now consider the coupled thermoelastic equations and with the quadratic element resolve the same problem. Fig. 10 shows the temperature distribution along the x-axis for $t=3$ and 6. At larger times, the temperature curve stays at higher values at larger x-values, due to the overall larger heat input. Fig. 11 is the distribution of the axial displacement along the x-axis at $t=3$ and $t=6$ for uncoupled ($C=0$) and coupled ($C=0.1$) equations. The coupled solution estimates lower curves for u with the wave fronts at $t=3$ and $t=6$. The curves start with compression at distance closer to the edge $x=0$, and tensile at over x-values. Fig. 12 is the distribution of the axial stress along the x-direction. The wave fronts for stress at time $t=3$ and $t=6$ are clearly shown in the figures, while the coupled solution underestimates the peak stress values. Due to unloading axial compression stress at distances close to the edge $x=0$, is developed.
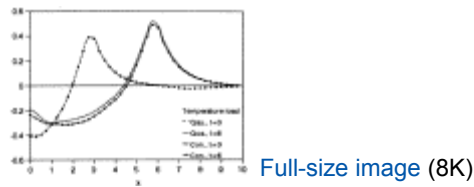
Full-size image (8K)

Fig. 7.

Comparison of the dimensionless temperature at middle of the plate for temperature loading.
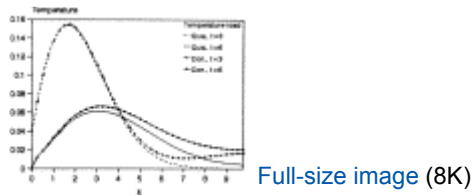

Full-size image (8K)

Fig. 8.

Comparison of the dimensionless axial displacement at middle of the plate for temperature loading.
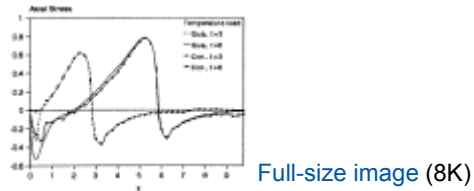

Full-size image (8K)

Fig. 9.

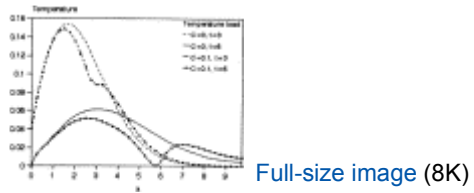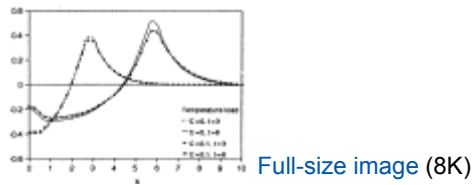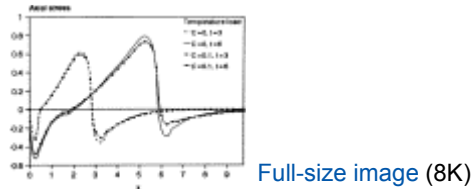Comparison of the dimensionless axial stress at middle of the plate for temperature loading.
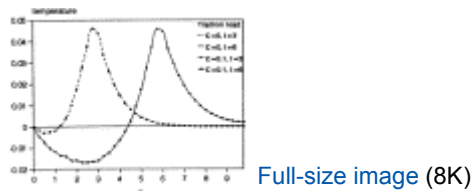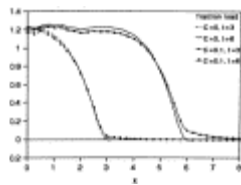

Full-size image (8K)

Fig. 10.

Comparison of the dimensionless temperature at middle of the plate for temperature loading.

Full-size image (8K)

Fig. 11.

Comparison of the dimensionless axial displacement at middle of the plate for temperature loading.

Full-size image (8K)

Fig. 12.

Comparison of the dimensionless axial stress at middle of the plate for temperature loading.

2. *Pressure shock alone:* The pressure shock of Eq. (24) is applied to the edge $x=0$ in the positive x-direction, and the coupled solution with quadratic elements are considered. Fig. 13shows the temperature distribution of the coupled solution for $C=0.1$ at times $t=3$ and $t=6$. Due to the coupled effect, even though the mechanical traction is applied, temperature rise is expected. The magnitude of the temperature distribution is, however, small. As is shown in Fig. 13, the peak of the temperature distribution curve is moved with the peak of the compressive stress along the x-axis. This phenomenon is observed due to the temperature induced by compressive stress as a result of the pressure shock. Fig. 14is the distribution of the axial displacement along the x-axis at $t=3$ and $t=6$ for uncoupled ($C=0$) and coupled ($C=0.1$) equations. The coupled solution estimates lower values for u. The wave fronts at $t=3$ and $t=6$ are clearly shown in the figure. Fig. 15shows the distribution of the axial stress along the x-axis. The stress wave front at $t=3$ and 6 is clearly observed. The coupled solutions are underestimated. The effect of the coupling is more evident at larger times.
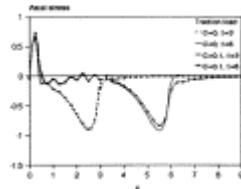

Full-size image (8K)

Fig. 13.

Comparison of the dimensionless temperature at middle of the plate for traction loading.

Full-size image (8K)

Fig. 14.

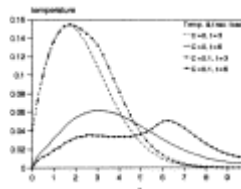Comparison of the dimensionless axial displacement at middle of the plate for traction loading.

Full-size image (7K)

Fig. 15.

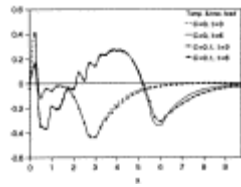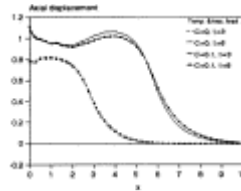Comparison of the dimensionless axial stress at middle of the plate for traction loading.

3. *Thermal and pressure shock in combination:* Now it is assumed that the mechanical pressure and temperature of (23) and (24) are applied simultaneously at the edge $x=0$. The axial displacement, temperature, and the axial stress along the x-axis are shown in Fig. 16, Fig. 17 and Fig. 18. A close study of the curves indicate that the results are the superimposed results of the cases (1) and (2) above, as expected. The interaction of the mechanical and thermal shock loads is shown to result into about 50% reduction in the compressive stress around the stress wave front. This can be verified by the comparison of Fig. 12 and Fig. 15 with Fig. 18.

Full-size image (8K)

Fig. 16.

Comparison of the dimensionless temperature at middle of the plate for temperature and traction loading.
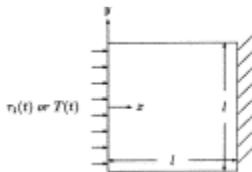
Full-size image (8K)

Fig. 17.

Comparison of the dimensionless axial displacement at middle of the plate for temperature and traction loading.
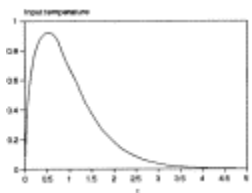

Full-size image (7K)

Fig. 18.

Comparison of the dimensionless axial stress at middle of the plate for temperature and traction loading.

Full-size image (3K)

Fig. 5.

A square plate subjected to thermal loading.

Full-size image (5K)

Fig. 6.

Pattern of thermal loading.

6. Conclusions

The conclusions of the paper may be expressed in the following areas:

1. Due to the short time periods of the applied mechanical and thermal shocks, the study of the coupled thermoelastic problems is critical at very short time periods after the shock applications. In this paper a hybrid BEM with Laplace transform in time domain is used and the structure behavior under coupled thermoelastic loading is studied at very small times without any need for the discretization of the domain.

2. The principal solution required for the boundary element formulation is derived for the coupled thermoelastic field.

3. The thermomechanical coefficient for the material under study is $C=0.01$. The reason to select $C=0.1$ is to clearly show the difference between the two theories.

4. The natural frequency of the two-dimensional domain considered for the example problem is much larger than the shock time period. As the result, when shocks are applied and removed, the after shock stress vibrations are incurred in the plate, as seen in Fig. 12, Fig. 15 and Fig. 18.

This paper is aimed to study the behavior of the plate under mechanical and thermal shocks. While the formulations are derived for a real two-dimensional finite domain, the results in this paper are reported for small time duration. Therefore, the wave reflections are not observed in the resulting figures. Since the importance of the coupled thermoelastic solutions are at short time periods after the shock applications, the response of the plate is obtained at early stages of the shock loads. However, time may be advanced as much as required and the behavior of the system may be studied at larger times [16].

References

[1] V.I. Danilovskaya, Thermal stresses in an elastic half-space due to a sudden heating of its boundary. *Prikl Mat Mekh*, **14** (1950), pp. 316–318.

[2] V.I. Danilovskaya, On a dynamic problem of thermoelasticity. *Prikl Mat Mekh*, **16** (1952), pp. 341–344.

[3] E. Sternberg and J.G. Chakravorty, On inertia effects in a transient thermoelastic problem. *ASME J Appl Mech*, **26** (1959), pp. 503–509.

[4] B.A. Boley and I.S. Tolins, Transient coupled thermoelastic boundary value problems in the half-space. *ASME J Appl Mech*, **29** (1963), pp. 637–646.

[5] R.E. Nickell and J.J. Sackman, Approximate solutions in linear, coupled thermoelasticity. *ASME J Appl Mech*, **35** (1968), pp. 255–266.

[6] F.J. Rizzo and D.J. Shippy, An advanced boundary integral equation method for three-dimensional thermoelasticity. *Int J Numer Meth Engng*, **11** (1977), pp. 1753–1768.

[7] M. Tanaka, H. Togoh and M. Kikuta, Fracture mechanics application in thermoelastic states, *Topics in boundary element research*, **Vol. 1** ,in: C.A. Brebbia, Editor, Springer, Berlin (1984) (chap. 3).

[8] V. Sladek and J. Sladek, Boundary integral equation method in thermoelasticity. Part I: general analysis. *Appl Math Modelling*, **7** (1984), pp. 241–253.

[9] I.G. Suh and N. Tosaka, Application of the boundary element method to 3-D linear coupled thermoelasticity problems. *Theor Appl Mech*, **38** (1989), pp. 169–175.

[10] S. Ishiguro and M. Tanaka, Analysis of two-D transient thermoelasticity by the time stepping BEM (in consideration of coupling effect). *Trans Jpn Soc Mech Engng, Ser A*, **59** (1993), pp. 2593–2598.

[11] G.F. Dargush and P.K. Banergee, A new boundary element method for three-dimensional coupled problems of conduction and thermoelasticity. *ASME J Appl Mech*, **58** (1991), pp. 28–36.

[12] L.G. Hector and W.S. Kim, Propagation and reflection of thermal waves in a finite medium due to axisymmetric surface sources. *Int J Heat Mass Transfer*, **4** (1992), pp. 897–912.

[13] P. Wagner, Fundamental matrix of the system of dynamic linear thermoelasticity. *J Thermal Stresses*, **17** (1994), pp. 549–569.

[14] J. Chen and G.F. Dargush, BEM for dynamic proelastic and thermoelastic analysis. *J Solids Struct*, **32** 15 (1995), pp. 2257–2278.

[15] P. Hosseini Tehrani and M.R. Eslami, Two-D time harmonic dynamic coupled thermoelasticity analysis by BEM formulation. *Engng Anal B E*, **22** (1998), pp. 245–250.

[16] P. Hosseini Tehrani and M.R. Eslami, Boundary element analysis of coupled thermoelastic problem with relaxation times in a finite domain, . *AIAA J*, (2000) (in press).

[17] Tosaka N. Boundary integral equation formulations for linear coupled thermoelasticity. Proc Third Japan Symp on BEM Jascome, Tokyo, p. 207–12..

[18] F. Durbin, Numerical inversion of Laplace transforms: an efficient improvement to Dubner and Abate's method. *Computer J*, **17** (1974), pp. 371–376.

Corresponding author. Tel.: +98-21-640-5844; fax: +98-21-641-19736

Home   Browse   Search   My settings   My alerts   Shopping cart

About ScienceDirect
What is ScienceDirect
Content details
Set up
How to use
Subscriptions
Developers

Contact and Support
Contact and Support

About Elsevier
About Elsevier
About SciVerse
About SciVal
Terms and Conditions
Privacy policy
Information for advertisers